ISSN 1063-7826, Semiconductors, 2016, Vol. 50, No. 12, pp. 1600–1603. © Pleiades Publishing, Ltd., 2016.
Original Russian Text © G.E. Fedorov, T.S. Stepanova, A.Sh. Gazaliev, I.A. Gaiduchenko, N.S. Kaurova, B.M. Voronov, G.N. Goltzman, 2016, published in Fizika i Tekhnika Poluprovodnikov, 2016, Vol. 50, No. 12, pp. 1625–1628.

XX INTERNATIONAL SYMPOSIUM "NANOPHYSICS AND NANOELECTRONICS", NIZHNY NOVGOROD, MARCH 14–18, 2016

Asymmetric Devices Based on Carbon Nanotubes for Terahertz-Range Radiation Detection

G. E. Fedorov*, T. S. Stepanova, A. Sh. Gazaliev, I. A. Gaiduchenko, N. S. Kaurova, B. M. Voronov, and G. N. Goltzman

Moscow State Pedagogical University, pr. Vernadskogo 88, Moscow, 119991 Russia

**e-mail: gefedorov@mail.ru*

Submitted April 27, 2016; accepted for publication May 10, 2016

Abstract—Various asymmetric detecting devices based on carbon nanotubes (CNTs) are studied. The asymmetry is understood as inhomogeneous properties along the conducting channel. In the first type of devices, an inhomogeneous morphology of the CNT grid is used. In the second type of devices, metals with highly varying work functions are used as the contact material. The relation between the sensitivity and detector configuration is analyzed. Based on the data obtained, approaches to the development of an efficient detector of terahertz radiation, based on carbon nanotubes are proposed.

DOI: 10.1134/S106378261612006X

1. INTRODUCTION

The applicability of carbon nanomaterials as the basis of the sensing element of terahertz-radiation detectors is due to a number of features of their characteristics. The case in point is mainly the high carrier mobility, the possibility of changing the properties by the gate voltage and the effect of geometrical sizes on the band-structure parameters. The results obtained to date [1–6] indicate the prospects of this direction of research from the viewpoint of obtaining practical results.

In this work, we study various asymmetric detecting devices based on carbon nanotubes (CNTs). A dc voltage signal appears in such devices upon exposure to electromagnetic radiation. Thus, they represent detectors operating at zero bias current. The devices under study are made in the field-effect transistor configuration, in which a lateral CNT array (CNT grid) or an individual CNT is a conducting channel. The asymmetry is understood as heterogeneous properties along the conducting channel. In the first device type, a heterogeneous morphology of the CNT grid is used. In the second device type, metals with greatly varying work functions are used as the contact material.

2. EXPERIMENTAL

Our devices are field-effect transistors with a conducting channel shaped as a CNT grid synthesized by chemical vapor-phase deposition [7]. The CNT-based sensing element is connected to a logarithmic spiral antenna whose arms represent dc contacts. When fabricating the first-type devices, one of the electrodes is connected to the CNT grid region placed on a catalytic island over the substrate; another electrode is connected to the CNT grid region placed directly on the substrate. When fabricating the second-type device, the antenna arms were made of different metals. In this case, CNTs (individual or grids) entirely arranged on the substrate were used as a channel. KDB-12 silicon coated with a thermal silicon oxide 250–500 nm thick was used as the substrate. The silicon substrate was used as a gate electrode; in this case, a gate voltage V_G was applied between the substrate and one of the antenna electrodes. The schematic diagram of both device types is shown in Fig. 1.

3. EXPERIMENTAL RESULTS

3.1. Experimental Setup

For better matching with radiation, the samples were fixed to the flat surface of a silicon lens. The lens and sample mounted on a copper holder were placed within a helium cryostat with a polytetrafluoroethylene (PTFE) optical window. A backward wave tube (BWT) with a maximum power of 800 μW at a frequency of 140 GHz was used as the sub-THz radiation source. The radiation power was varied using a grid attenuator. The response to amplitude-modulated radiation (with a modulation frequency from 100 Hz to 100 kHz) was measured using a lock-in amplifier.

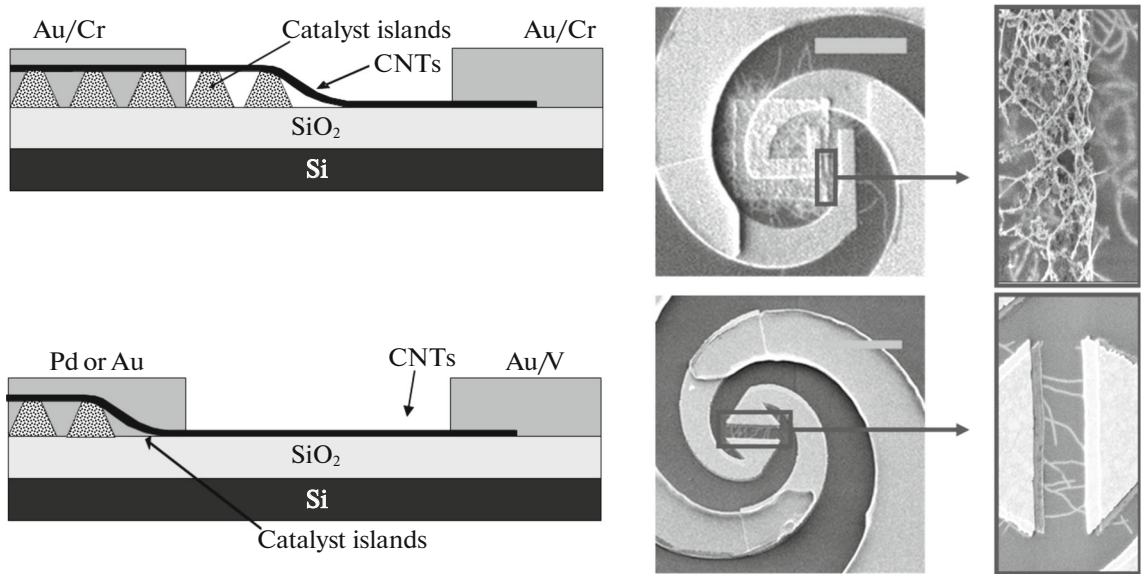

Fig. 1. Configuration of the first- and second-type devices. The top panel shows the schematic diagram of the sensing element; the right panel shows the SEM micrograph of the first-type sample. The bottom panel shows the same for the second-type samples. The scale bars in the SEM micrographs correspond to a size of 10 μm.

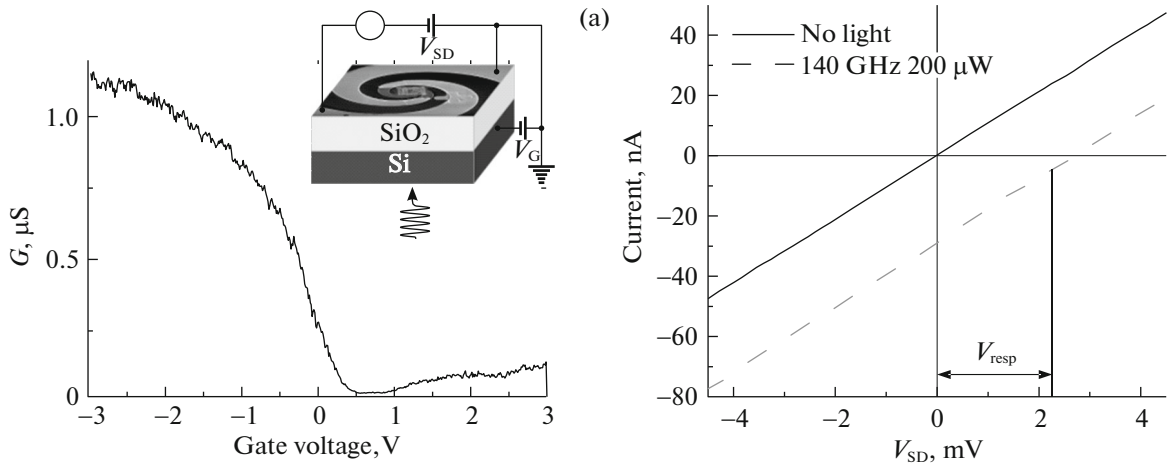

Fig. 2. (a) Transfer characteristic of the device with a conducting channel based on an individual semiconductor CNT. The inset shows the device connection circuit diagram. (b) Modification of the *I–V* characteristic of the first-type device upon exposure to radiation.

The current–voltage (*I–V*) characteristics of the samples were measured using a Keithley 2400 SourceMeter. The electrical connection circuit of the sample is shown in Fig. 2a. All results presented below were obtained at room temperature.

3.2. Sample Characterization Results

The dependence of the device conductance on the gate makes it possible to identify the channel-conductance type. Figure 2b shows the device transfer characteristic in which an individual semiconductor CNT is a conducting channel. The response of samples under study to radiation is illustrated in Fig. 2b showing *I–V* characteristics of the second-type sample, measured in the dark mode upon exposure to radiation with a frequency of 140 GHz. The radiation power incident on the silicon lens outer surface is ~200 μW. As seen in Fig. 2b, the *I–V* characteristic shifts along the voltage axis upon exposure to radiation. The bias voltage at zero current, denoted as V_{resp}, is several mV; in this case, the differential conductance remains unchanged. The ratio of the response voltage to the power, referred to as the volt–watt sensitivity, is one of the key parameters defining the detector-operation efficiency. In the

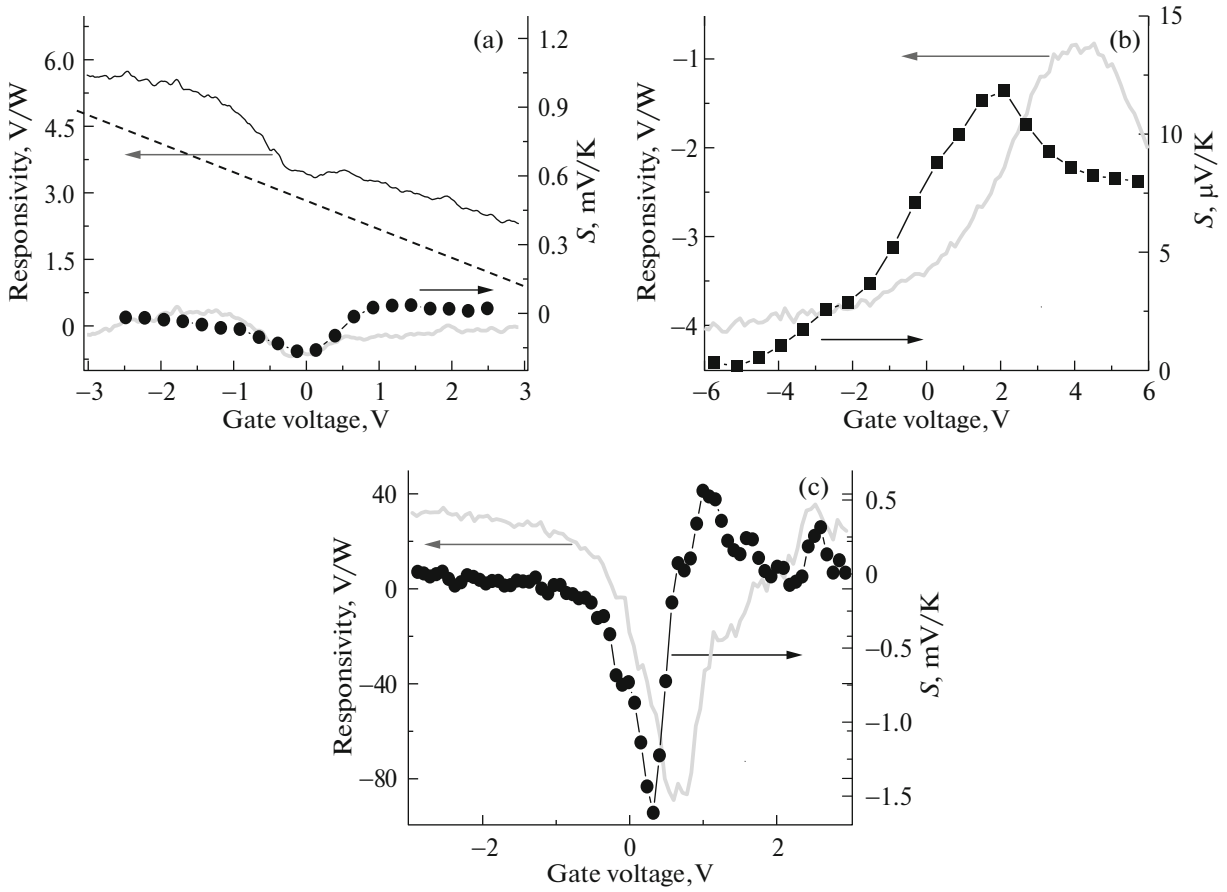

Fig. 3. (a) Dependence of the volt–watt sensitivity and the Seebeck coefficient calculated according to formula (1) on the gate voltage for devices of various configurations. (a) The first-type sample. The gray curve is the result of subtraction of the linear background (dashed line) from the dependence of the volt–watt sensitivity on the gate. (b) The second-type sample with a CNT grid. (c) The second-type sample with an individual semiconductor CNT.

experiments described, it is from several to several tens of V/W.

3.3. Study of the Device Response

To identify the physical mechanisms causing the observed response, we studied its dependence on the gate voltage. Figure 3 shows the data obtained for three samples of different configurations, i.e., the dependences of the volt–watt sensitivity (the ratio of the response voltage to the incident radiation power) for the first-type sample (Fig. 3a), the second-type sample based on a CNT grid (Fig. 3b), and the second-type sample based on an individual semiconductor CNT (Fig. 3c). We immediately note that the highest volt–watt sensitivity is observed for the third sample. An important feature of the response is its nonmonotonic dependence on the gate voltage.

In Fig. 3, the dependences of the response on the gate voltage are compared with the derivative of the conductance logarithm with respect to the gate voltage. Such a comparison allows the separation of the contribution of the so-called photothermoelectric effect which is related first of all to the temperature nonuniformity along the channel. As a result of the interaction of electromagnetic radiation with the electronic subsystem of the conducting channel, the electron temperature increases above the phonon temperature. In the first-type devices, carrier thermalization is less efficient in the CNT grid region which is on a catalytic island over the substrate, in comparison with that in direct contact with the substrate. In the second-type devices, the difference in the contact resistance at the CNT–metal interface leads to different heating of the near-contact regions due to Joule heat release during radiation-induced ac current flow.

Thus, radiation causes nonuniform heating of the conducting channel in all the devices under study, and thermopower appears between electrodes. It is calculated as the product of the temperature difference and the so-called Seebeck coefficient S, which can be cal-

culated in the diffusion transport approximation according to the formula [8]

$$S \equiv \frac{\Delta V}{\Delta T} = -\frac{\pi^2 k_B^2 T}{3|e|}\frac{1}{G}\frac{dG}{dE}\Big|_{E_F} = \frac{\pi^2 k_B^2 T}{3|e|}\frac{1}{G}\frac{dG}{dV_G}\frac{dV_G}{dE}\Big|_{E_F}, \quad (1)$$

where k_B is the Boltzmann constant, e is the elementary charge, and E is the energy measured from the Fermi level. The last factor dV_G/dE can be estimated as $10/e$ [8]. The form of the dependences $S(V_G)$ calculated by this formula is in general identical to the dependences of the response on the gate voltage. In this case, while $S(V_G)$ tends to zero at gate voltages that are higher in magnitude, the response either tends to a constant nonzero value or steadily decreases as a function of the gate voltage (see Fig. 3a), which is especially pronounced in the region of negative V_G.

The above features of the dependences $V_{resp}(V_G)$ indicate the existence of the another mechanism of dc-voltage appearance. The asymmetry inherent to our devices should lead to two effects which in general can cause the experimentally observed dc voltage signal. The first thermal effect is due to the appearance of the temperature gradient in the transistor channel upon exposure to radiation. The second effect is associated with the nonlinearity of the I–V characteristic and is called the diode effect.

The diode response is calculated using the formula (see [9])

$$S_V = -\frac{1}{4}\frac{d^2 I}{dV^2} R_S Z_A, \quad (2)$$

where R_S is the device resistance and Z_A is the antenna impedance equal to 75 Ω. For all samples, the calculation of the volt–watt sensitivity according to formula (2) using the transport characteristics (the resistance and the second derivative of current with respect to voltage), measured at a gate voltage of 3 V, yields a value about twice the experimental value. Thus, this approximation adequately describes the obtained values of the volt–watt sensitivity.

A comparison of the data obtained using samples of various configurations shows that the second-type sample with a conducting channel formed by a semiconductor CNT exhibits the highest volt–watt sensitivity. The mode corresponding to the negative gate voltage, when the channel is doped with p-type carriers, is better for practical applications. It is important to note the principal possibility of doping CNTs due to noncovalent functionalization of their surface, which makes it possible not to use the gate electrode. To improve the stability of the detector characteristics, it is more preferable to use not individual CNTs, but their lateral arrays where up to several tens of CNTs are connected in parallel. As seen from the data obtained in this study, such structures have a lower sensitivity. This is most likely associated with the presence of metal CNTs in such arrays (their number should be about 1/3 of the total number of CNTs in an array [10]). However, there are procedures of CNT synthesis by chemical vapor-phase deposition that allow the production of up to 99% of semiconductor CNTs [11]. A combination of these methods with the approaches described in this paper would possibly allow the development of a new class of energy-efficient and sensitive detectors of THz radiation based on CNTs.

4. CONCLUSIONS

Asymmetric structures based on carbon nanotubes are of interest for the development of terahertz-radiation detectors. The results presented in this paper show the promising application of a lateral array of semiconductor CNTs as a detector sensing element, the contact to which is implemented using metals with different work functions.

ACKNOWLEDGMENTS

This study was supported by the Ministry of Education and Science of the Russian Federation (agreement no. 14.586.21.0003, unique identifier RFMEFI58614X0003).

REFERENCES

1. X. He, N. Fujimura, J. M. Lloyd, K. J. Erickson, A. A. Talin, Q. Zhang, W. Gao, Q. Jiang, Y. Kawano, R. H. Hauge, F. Leonard, and J. Kono, Nano Lett. **14**, 3953 (2014).
2. X. He, F. Lonard, and J. Kono, Adv. Opt. Mater. **3**, 989 (2015).
3. L. Vicarelli, M. S. Vitiello, D. Coquillat, A. Lombardo, A. C. Ferrari, W. Knap, M. Polini, V. Pellegrini, and A. Tredicucci, Nat. Mater. **11**, 865 (2012).
4. X. Cai, A. B. Sushkov, R. J. Suess, M. M. Jadidi, G. S. Jenkins, L. O. Nyakiti, R. L. Myers-Ward, S. Li, J. Yan, D. K. Gaskill, T. E. Murphy, H. D. Drew, and M. S. Fuhrer, Nat. Nanotechnol. **9**, 814 (2014).
5. G. Fedorov, A. Kardakova, I. Gayduchenko, I. Charayev, B. M. Voronov, M. Finkel, T. M. Klapwijk, S. Morozov, M. Presniakov, I. Bobrinetskiy, R. Ibragimov, and G. Goltsman, Appl. Phys. Lett. **103**, 181121 (2013).
6. I. Gayduchenko, A. Kardakova, G. Fedorov, B. Voronov, M. Finkel, D. Jimenez, S. Morozov, M. Presniakov, and G. Goltzman, J. Appl. Phys. **118**, 194303 (2015).
7. A. Tselev, K. Hatton, M. S. Fuhrer, M. Paranjape, and P. Barbara, Nanotechnology **15**, 1475 (2004).
8. J. Small, K. Perez, and P. Kim, Phys. Rev. Lett. **91**, 256801 (2003).
9. K. Fu, R. Zannoni, C. Chan, S. H. Adams, J. Nicholson, E. Polizzi, and K. S. Yngvesson, Appl. Phys. Lett. **92**, 033105 (2008).
10. R. Saito. G. Dresselhaus, and M. S. Dresselhaus, *Physical Properties of Carbon Nanotubes* (Imperial College Press, London, 1998).
11. L. Ding, A. Tselev, J. Wang, D. Yuan, H. Chu, T. P. McNicholas, Y. Li, and J. Liu, Nano Lett. **9**, 800 (2009).

Translated by A. Kazantsev